WILEY-VCH

Photo-induced self-cleaning and wettability in TiO_2 nanocolumn arrays obtained by glancing-angle deposition with sputtering

Fernando Fresno, María U. González, Lidia Martínez, Marcial Fernández-Castro, Mariam Barawi, Ignacio J. Villar-García, Jimena Soler-Morala, Patricia Reñones, Mónica Luna, Yves Huttel,* Víctor A. de la Peña O'Shea,* José M. García-Martín**

Dr. F. Fresno, Dr. M. Barawi, Dr. I. J. Villar-García, Dr. P. Reñones, Dr. V. A. de la Peña O'Shea
Photoactivated Processes Unit, IMDEA Energy, Avda. Ramón de la Sagra, 3, 28935 Móstoles, Madrid, Spain
E-mail: fernando.fresno@imdea.org; victor.delapenya@imdea.org

Dr. María U. González, M. Fernández-Castro, J. Soler-Morala, Dr. M. Luna, Dr. J. M. García-Martín
Instituto de Micro y Nanotecnología, IMN-CNM, CSIC (CEI UAM+CSIC), Isaac Newton 8, 28760 Tres Cantos, Madrid, Spain
E-mail: josemiguel.garcia.martin@csic.es

Dr. L. Martínez, Dr. Y. Huttel
Materials Science Factory, Instituto de Ciencia de Materiales de Madrid, ICMM-CSIC, Sor Juana Inés de la Cruz 3, 28049 Madrid, Spain
E-mail: huttel@icmm.csic.es

Keywords: TiO_2, nanocolumns, metal nanoparticles, magnetron sputtering, photocatalysis, photoinduced hydrophilicity, self-cleaning

Abstract

In this work, we report on the preparation of regular nanosized columnar structures of titanium dioxide by means of glancing angle deposition with magnetron sputtering (MS-GLAD) followed by thermal annealing. MS-GLAD gives rise to metallic titanium columnar structures with regular width and length that after thermal treatment are fully oxidized to form TiO_2 nanocolumns that fairly maintain the morphological features of the original metallic ones. Further functionalization with gold by means of multiple ion cluster source results in well-dispersed Au nanoparticles across the nanocolumns surface with a narrow size distribution centered at ca. 8.5 nm. The obtained nanostructures show photocatalytic self-cleaning activity as shown by the elimination of an organic layer deposited on their surface and the detection of hydroxyl radicals. Photoelectrochemical measurements have shown a better charge separation at the Au/TiO_2 interface. In addition, wettability studies have shwon that the degree of hydrophobicity of the surface is increased by the presence of nanocolumns, both in the dark and under UV illumination. This behaviour is not modified by the presence of Au nanoparticles on the surface. The obtained results open up interesting implications in the tunability of the properties of nanostructured thin films for this kind of photo-activated applications.

1. Introduction

Titanium dioxide (TiO_2) is one of the most interesting materials nowadays with a plethora of technological applications, from the most developed ones like additive in pharmaceuticals, catalyst support, or white pigment, to the most challenging ones like the production of solar fuels and the electrochemical energy storage in lithium or sodium ion batteries.[1–3] Light-activated applications of TiO_2 make use of its semiconducting nature and rely on the generation of electron-hole pairs upon irradiation with appropriate wavelengths. These applications stand out among the most relevant ones in research and with the greatest technological projection. Thus, TiO_2-based solar cells,[4] photocatalytic pollutant removal from water[5] and air,[6] photoinduced hydrophilicity,[7] and the obtainment of solar fuels in photocatalytic reactors[8] and photoelectrochemical cells,[9] are extensively studied today, with variable degree of maturity depending on the case, for an efficient use of solar light in energy and environmental applications.[10]

Self-cleaning and anti-fogging technology is already used in a variety of products today, among which glazing products prevail. Their function may be based on two principles, either hydrophobicity (Lotus effect), or photocatalytic hydrophilicity.[11,12] In the latter case, the self-cleaning action is based on the combination of photocatalysis and photoinduced superhydrophilicity, where dirt removal by uniform spreading of water over the whole surface is improved with photocatalytic decomposition of organic contaminants.[13,14] Furthermore, the oxidative character of photogenerated holes in TiO_2 allows to extend the application of photocatalytic films to the disinfection of surfaces through the inactivation of bacteria and viruses,[15,16] potentially including the pandemic-causing SARS-CoV-2 coronavirus.[17,18]

In spite of the high readiness level of this technology, with competitive products already in the market, there is room to improve the properties and extend the applications of self-cleaning and anti-fogging surfaces by designing and tailoring new nanoarchitectures for light-

activated thin films.[19] In the particular case of TiO_2, considering that it gathers nearly all the desired characteristics of a photocatalyst, the interest on the synthesis and applications of titania 1D and 2D structures such as nanorods, nanowires and nanotubes has increased in the last decades due to their singular properties in terms of surface area, charge separation and transport, and tunability.[20] In particular, glancing angle deposition with magnetron sputtering (MS-GLAD) is a powerful technique for producing nanostructured coatings in large areas and with a great variety of morphologies.[21–23] In this work, we have followed our recent protocol to fabricate TiO_2 nanocolumn arrays in two steps: growth of Ti nanocolumns (NCs) by MS-GLAD and subsequent thermal oxidation to transform them into TiO_2.[24]

In addition, further modification of TiO_2 photoinduced properties can be achieved by creating a semiconductor-metal interface by means of metal nanoparticle decoration, which provides the system with enhanced charge separation and can modify the surface chemistry, representing a powerful method to tune the characteristics of photoactive surfaces.[12,14] In particular, gold nanoparticles with sizes of a few nanometers have shown very interesting properties not only in photocatalysis but also in other catalytic and related applications.[25] The TiO_2 NCs obtained in this work have been further functionalized with ligand-free gold nanoparticles (Au NPs) by means of an ion cluster source (ICS) or gas aggregation source method.[26–29] Since the seminal work of Haberland and co-workers,[30] these sources have become a powerful alternative to chemical methods for the fabrication of nanoparticles.[31] In ICS, a solid material is atomized in vacuum and subsequently the atoms are condensed in a controlled manner in order to form nanoparticles of well-controlled mean size, chemical composition and narrow size distribution.[32–34] Among the different ways of extracting the atoms, the magnetron process has become very popular due to its versatility. In this work, a modified ICS called multiple ion cluster source (MICS) has been used. In the MICS the standard single magnetron is replaced by three independent magnetrons that allow the

production of a wide variety of nanoparticles including alloyed and core@shell nanoparticles in a single step.[26–29]

The so-obtained TiO_2NCs and AuNPs/TiO_2NCs have been submitted to extensive characterization, combined with photo-functional analysis by means of wettability measurements and photocatalytic degradation experiments, which has allowed to explore their potential application as tunable photoactive surfaces and the reasons behind their performance.

2. Results and discussion

2.1. Physico-chemical characteristics of columnar nanostructures

The initial metallic titanium NCs obtained by MS-GLAD are characterized by fairly regular columnar structures (Figs. 1a and 1c) of 265 nm average thickness in which columns of approximately 50 nm of diameter and 310 nm average length form an angle of 30° with respect to the direction normal to the substrate.

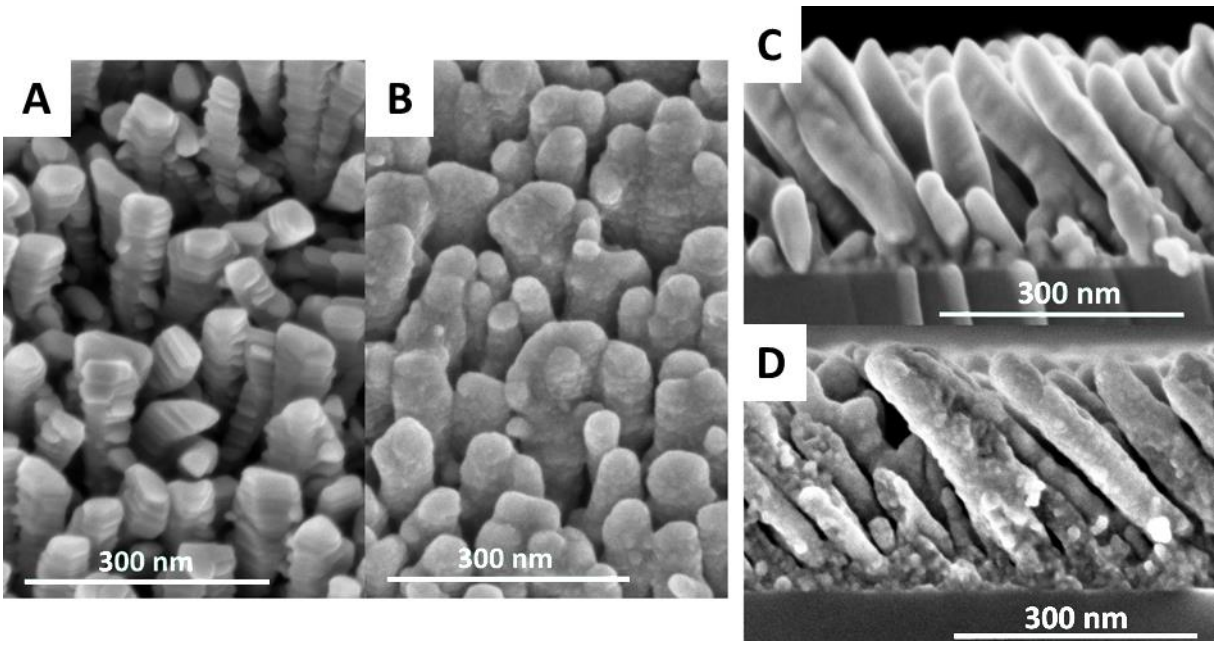

Figure 1. (A) Top view SEM image of Ti NCs. (B) top view SEM image of TiO_2 NCs oxidized at 500 ºC. (C) cross-section SEM image of Ti NCs and (D) cross-section SEM image of TiO_2 NCs oxidized at 500 ºC.

The X-ray diffraction (XRD) pattern (Fig. 2A) of initial metallic nanocolumns shows only reflections corresponding to the hexagonal close-packed (hcp) structure of metallic titanium, with the intensity distribution revealing certain preferential crystal orientation.[35] After

oxidation in an air stream at 500 °C, the structures are fully oxidized to TiO_2, mainly in the rutile crystalline form although the shoulder at ca. 25.5° reveals the existence of a minor amount of anatase phase. Additional low-intensity peaks can be ascribed to a minor amount of SiO_2 due to surface oxidation of the Si substrate. In situ diffraction measurements during the oxidation process (Fig. 2B) show that the metallic structures are stable until a temperature of ca. 400 °C is reached, at which diffraction signals corresponding to rutile start to grow while those of the hexagonal metallic phase decrease. From the evolution of the relative intensities, it is apparent that the transformation from Ti to TiO_2 proceeds directly to the rutile phase, without a transition through anatase, although the latter is always present in a minor amount. Alternatively, the transition through anatase might be too short in time to be observed by XRD. At the final temperature of 500 °C the intensities of the metallic phase have completely disappeared with only those corresponding to TiO_2 visible. A displacement due to temperature effects is finally observed during cool down to room temperature.

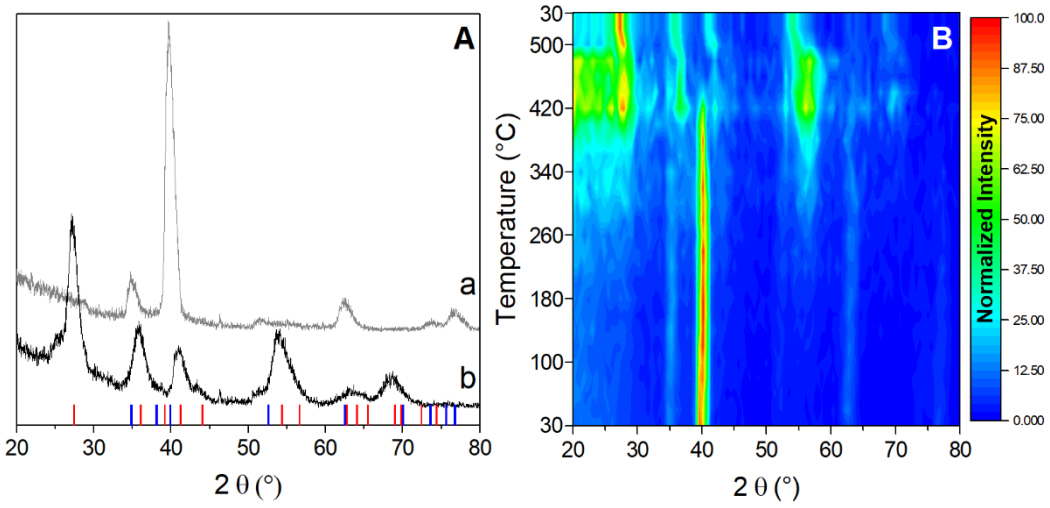

Figure 2. (A) X-ray diffractograms of initial Ti metal nanocolumns (a) and TiO_2 nanocolumns after oxidation in air at 500 °C (b). Blue and red bars indicate, respectively, the diffraction angles corresponding to Ti metal (ICDD PDF # 01-071-4632) and rutile TiO_2 (ICDD PDF # 01-072-1148). (B) Color map of in-situ X-ray diffraction during the oxidation process.

After the oxidation procedure the morphology of the nanocolumns underwent a modification towards wider and more interconnected columns (Figure 1 b and d). This can be ascribed to

the lower density of TiO_2 with respect to Ti metal, and the coalescence of some nanocolumns due to temperature effects, although the original morphology is essentially maintained.

Regarding Au NP formation, a typical AFM image and the obtained size distribution of model Au nanoparticles deposited on bare SiO_x substrates is shown in Figure S1. The histogram can be fitted to a log-normal distribution and the average height obtained was 8.1 ± 0.4 nm.

After the good control of size distribution of Au NPs was checked on bare SiO_x substrates, they were deposited onto the TiO_2 NCs. Figure 3 shows representative SEM images of the so-obtained Au-decorated TiO_2 nanocolumns. Images (a) and (c) were obtained using the standard detection of secondary electrons, whereas images (b) and (d) were obtained by collecting back-scattered electrons. As the signal collected with those back-scattered electrons depends of the atomic number, the Au nanoparticles can be easily distinguished with brighter contrast from the TiO_2 background.

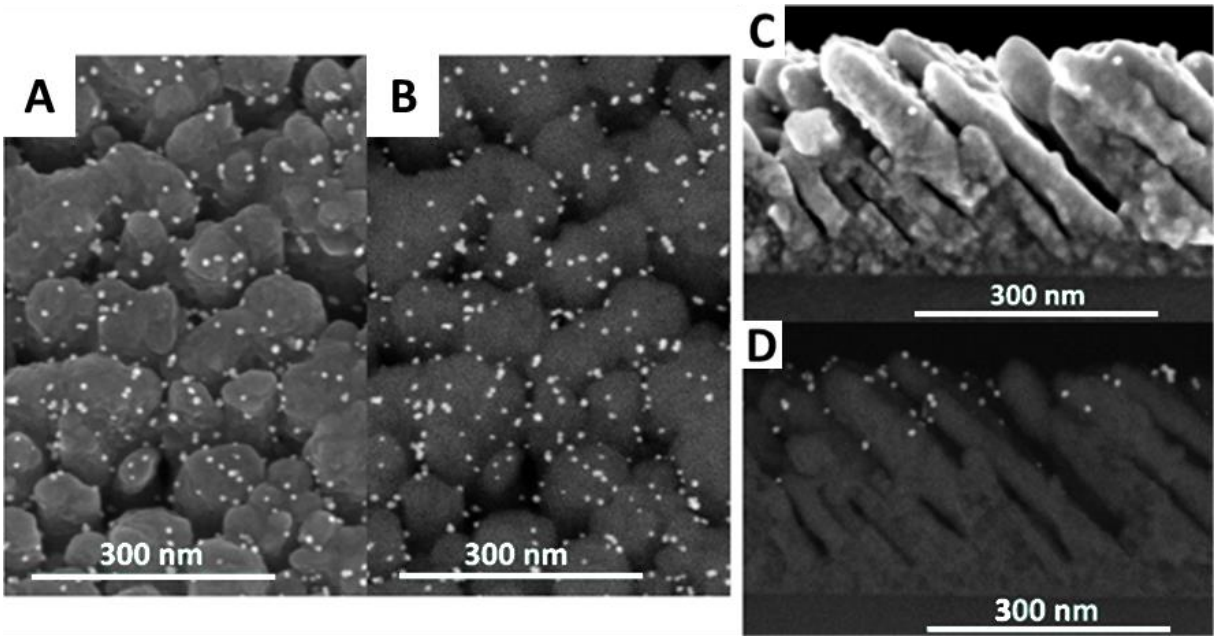

Figure 3. (A) Top view SEM image of Au NPs deposited on TiO_2NCs. (B) same image but detecting back-scattered electrons. (C) cross-section SEM image of AuNPs/TiO_2NCs. (D) same image but detecting back-scattered electrons. The back-scattered electrons give higher contrast, allowing to better discriminate the deposited Au NPs.

The nanoparticles lateral dimension was also measured using back-scattered electrons SEM images from different samples and different sample areas in order to have enough and broad

statistics. A total of 500 nanoparticles were measured on top of the TiO_2 nanocolumns and the histogram is shown in Figure 4. The average diameter obtained was 8.6 ± 2.5 nm, which is in good agreement with the AFM results of the model Au NPs, confirming that the TiO_2 nanocolumns obtained by MS-GLAD followed by thermal oxidation constitute an appropriate support for size-controlled metal nanoparticles, opening up extensive opportunities for further functionalization of the columnar structures.

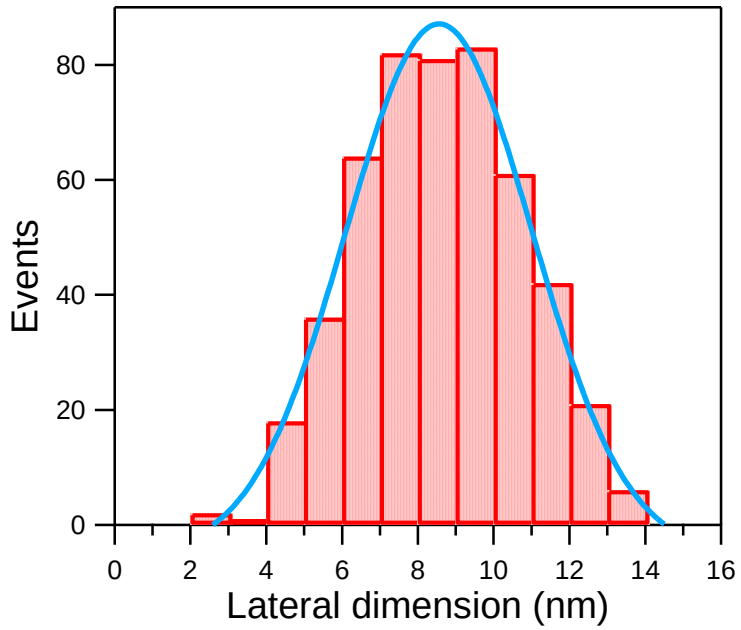

Figure 4. Histogram of Au NPs diameters obtained from back-scattered electrons SEM images.

X-ray photoelectron spectroscopy (XPS) analyses were performed on both TiO_2NCs and AuNPs/TiO_2NCs samples. Characteristic peaks for Ti, O and C can be seen in the survey scans of both samples (Figure S2), the scan of the AuNPs/TiO_2NCs sample also showing Au characteristic peaks. Si 2p scans were also taken in order to acquire a measurable area for peak quantification (Figure S3). The calculated atomic percentage for Si is below 3% for both samples, suggesting nearly full and homogenous surface coverage of the SiO_x substrate. The binding energy values observed for the $Ti2p_{3/2}$ (459.3 eV, Figure 5) and O1s (530.4 eV, Figure 5) peaks of both samples are characteristic of TiO_2.[36] The $Ti:O_{lattice}$ ratio is close to the stoichiometric 1:2 value for TiO_2, which confirms the total oxidation of the metallic

nanocolumns after the thermal treatment. The O1s peaks fitted at higher binding energies are characteristic of the typical hydroxyl groups and carbonates commonly found on the surface of TiO_2 samples that have been exposed to the atmosphere.[3] There is also a clear C1s peak at a binding energy characteristic of carbonate moieties in the C1s high resolution scan (Figure S4) with a 1:3 C:O ratio, confirming their presence on the sample. In the C1s scan there is also a signal contribution related to adventitious contamination containing oxygenated compounds such as carbonyls. These species might also contribute to the total intensity of the fitted O1s hydroxides and carbonate peaks. The Au $4f^{7/2}$ peak (Figure 5) has the characteristic peak shape, binding energy (84.0 eV) and full width at half maximum (below 1 eV) of fully metallic Au nanoparticles with sizes higher than 5 nm and in a charge-neutral, bulk like state, as seen in a detailed study by Jaramillo and co-workers,[25] in good agreement with the microscopy characterization data exposed above.

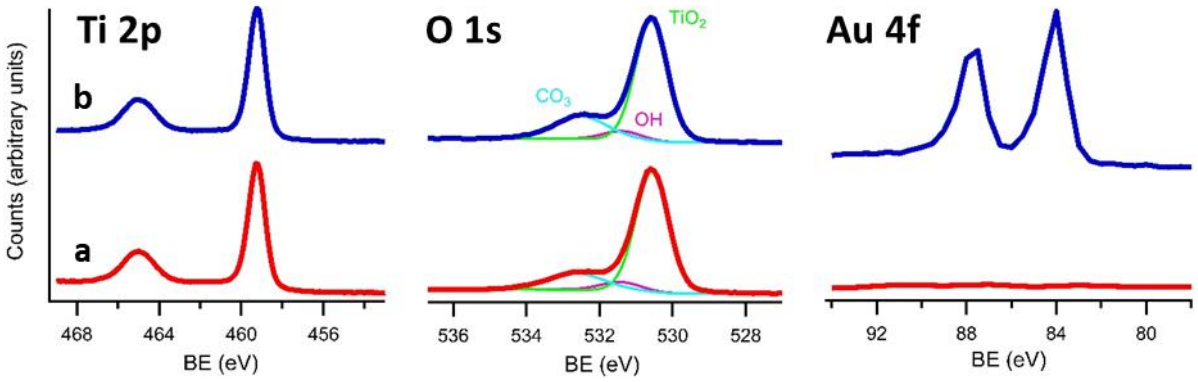

Figure 5. High-resolution X-ray photoelectron spectra of TiO_2NCs (a) and AuNPs/TiO_2NCs (b) samples at the Ti2p, O1s and Au4f core level peaks.

2.2. Photoinduced self-cleaning activity

The wettability properties of the samples were tested by measuring the water contact angle (CA) on their surface under UV irradiation. As shown in Figure 6, TiO_2NCs show an exponential decrease in the contact angle with irradiation time, from an initial CA of ~105º to ~65º after 130 min of UV irradiation, confirming a photoinduced hydrophobic-to-hydrophilic transition. There are different mechanisms proposed in the literature for this photoinduced

hydrophilicity, being the oxidative removal of organic contaminants or dissociative adsorption of water at the TiO_2 surface by UV light, which results in an increase of the surface hydroxyl groups, among the most accepted ones.[13] This hydrophilic nature of TiO_2 is known to enhance its photocatalytic self-cleaning performance.

However, in the case of TiO_2NCs, the initial CA is larger than the ones usually reported for TiO_2 films, close to 60º.[37,38] This effect can be attributed to nanostructuration, which can induce more hydrophobic surfaces.[39] Moreover, the CA under UV irradiation found for the TiO_2NCs sample is also considerably larger than the ones usually reported for TiO_2 films,[37,40] which likely results from the opposed effects of the roughness in the nanoscale provided by the nanocolumnar structures and the photoactive nature of TiO_2.

When the nanostructures are decorated with Au NPs, there is no significant variation of the CA measured. Before UV irradiation, a CA of ~115º evidenced that the presence of Au NPs has small influence on the wettability of the TiO_2NCs, even if Au is known to be hydrophilic. This can be related to the fact that Au NPs cover only a small percentage of the NCs surface (Figure 3). Under UV irradiation, a photo-induced hydrophobic-to-hydrophilic transition can also be observed, and the CA vs. time curve is approximately parallel to that of the bare TiO_2NCs sample, although a higher dispersion of data can be observed. This last feature can be related to a higher surface heterogeneity provoked by gold deposition, even if the coverage of TiO_2 NCs by Au NPs is fairly homogeneous (Figure 3). After the tested period of UV irradiation, a CA of ~60º is reached in AuNPs/TiO_2NCs, similar to that in bare TiO_2NCs considering the measurement uncertainty.

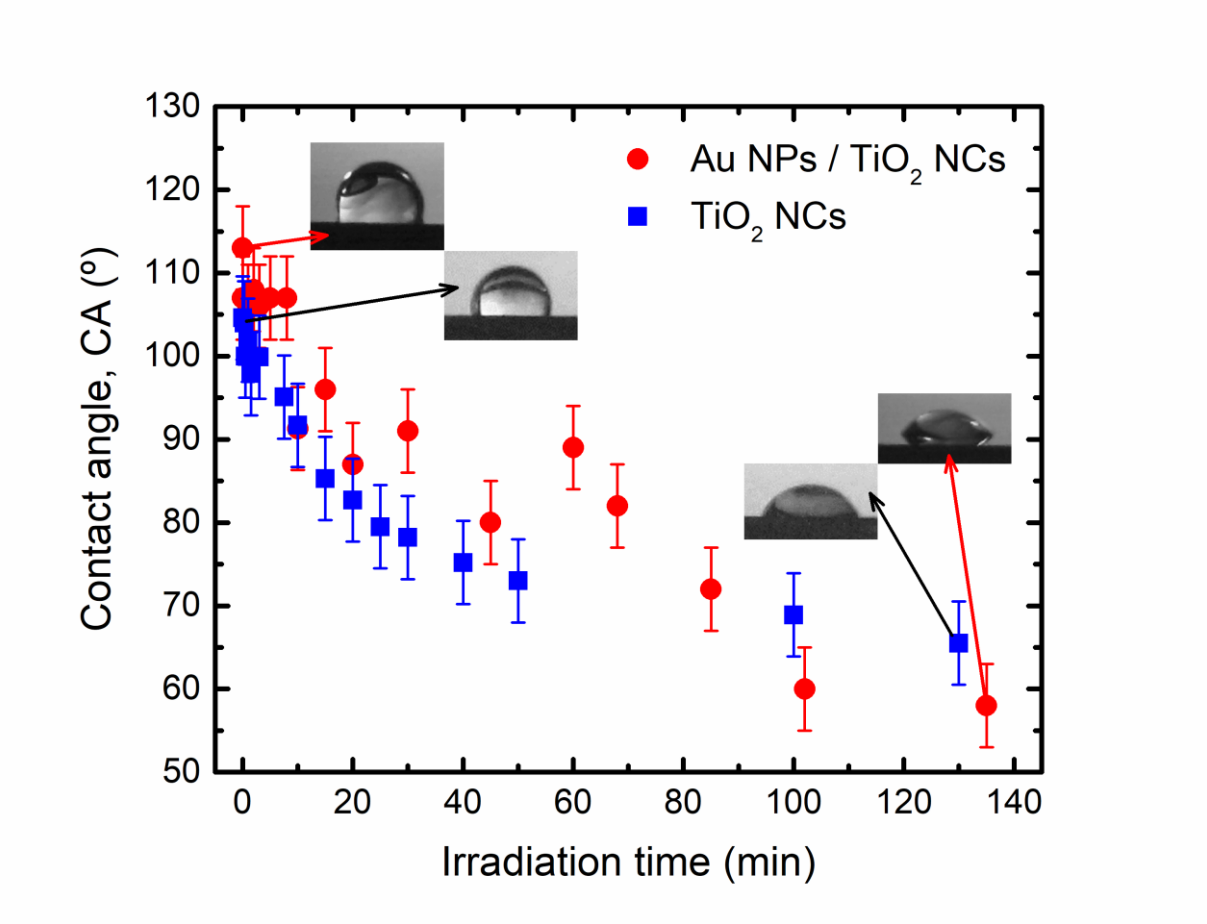

Figure 6. Evolution of water contact angle on bare and Au-decorated TiO_2 NCs with UV irradiation time.

In addition, photo-oxidative character was tested by the well-established method based on the degradation, by oxidation to CO_2 and H_2O, of a solid film of stearic acid (SA) as a model of the type of organic films that generate dirt on surfaces.[41,42] Figure 7 shows the infrared spectra, in the region corresponding to the C-H stretching vibrations, of both bare and Au-decorated TiO_2 NCs samples covered with a solid film of stearic acid after different UV irradiation times, as well as the evolution of the corresponding integrated absorbance. As it can be observed, both samples show a fast decrease in the SA signals, comparatively faster, for example, than that observed with the "reference" photocatalysis-based self-cleaning glass Pilkington Activ™.[43] As found in previous studies,[43,44] the degradation rate initially follows apparent zero-order kinetics and deviates from it when the remaining number of stearic acid molecules is not sufficient to replace the mineralized ones over the photocatalytically active

sites. In contrast with the previously shown wettability results, in this case the presence of gold nanoparticles decorating the nanocolumn surface leads to a higher photoactivity of the film as revealed by the faster stearic acid mineralization and the higher degree of degradation attained once a pseudo-steady state has been reached, ca. 60 and 70% for TiO_2NCs and AuNPs/TiO_2NC, respectively, with respect to the initial IR absorbance.

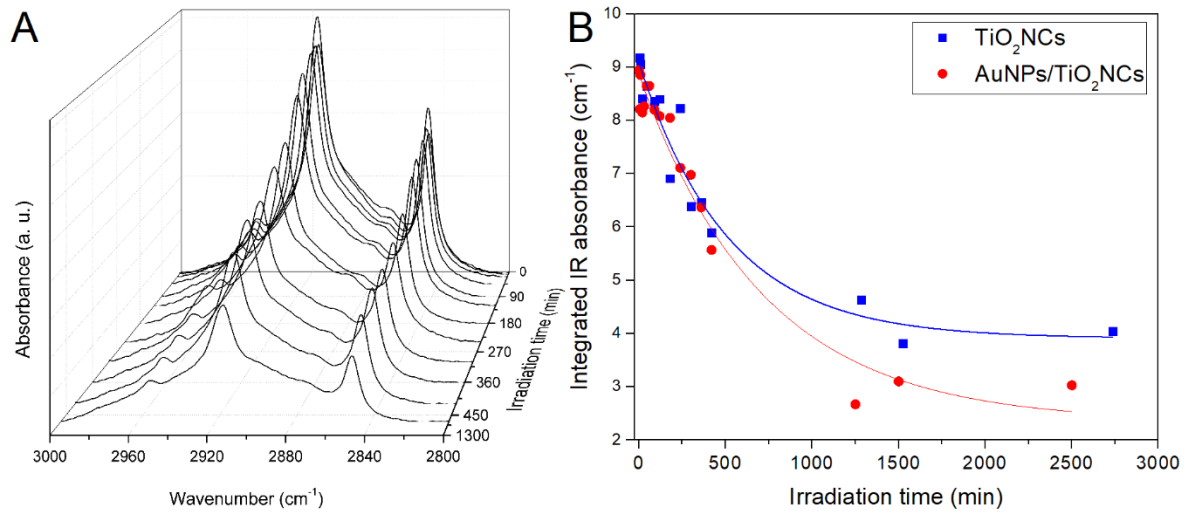

Figure 7. (A) Infrared spectra of a TiO_2NCs sample covered by a solid stearic acid film after different UV irradiation times. (B) Evolution of the integrated absorption in the 3000 – 2800 cm^{-1} region with irradiation time for TiO_2NCs and AuNPs/TiO_2NCs samples. Lines are guides to the eye only.

Taking into account that the oxidation of fatty acids and other organics on photocatalytically active surfaces likely occur through the intermediation of hydroxyl radicals,[44,45] ·OH detecting experiments were conducted to double-check the photocatalytic response of TiO_2NCs and AuNPs/TiO_2NCs films. For that purpose, the formation of hydroxyterephthalic acid (HTPA) from a solid terephthalic acid (TPA) film deposited on both samples was followed by fluorescence measurements.[46,47] The formation of HTPA from TPA can be described with Eq. (1):

$$[\mathrm{HTPA}] = \frac{k_1}{k_2}\left(1 - e^{-k_2 t}\right) \qquad (1)$$

where k_1 and k_2 represent, respectively, the zero-order kinetic constant for TPA hydroxylation and the first-order constant for HTPA disappearance to form further oxidation products and

eventually CO_2. Figure 8 shows the evolution of HTPA on both samples and the corresponding k_1 values, which reflect the higher activity obtained for the gold-decorated sample also in this reaction, confirming, on the one hand, the oxidizing character of the titania nanocolumn film and, on the other hand, the role of the metal nanoparticles as photocatalytic activity promoter.

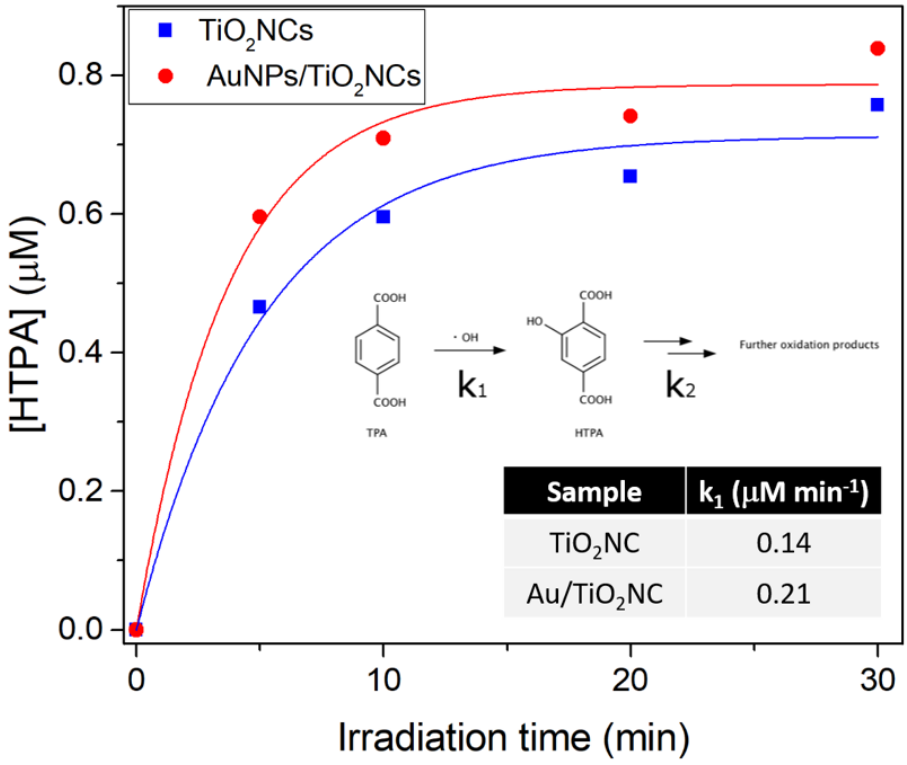

Figure 8. Evolution with irradiation time of the concentration of hydroxyterephthalic acid formed by hydroxylation of terephthalic acid over TiO_2NCs and Au NPs/TiO_2NCs. The red line corresponds to the fitting of the concentration vs. time data to Eq. 1 according to the inset reaction, with obtained k_1 values shown in the inset table.

2.3. Photoelectrochemical response

In order to further investigate the optoelectronic properties responsible for their photocatalytic behavior, several electrodes were prepared with the TiO_2NCs and AuNPs/TiO_2NCs samples and used in a photoelectrochemical cell coupled to a solar simulator. Figure 9A presents the measured photovoltage signal obtained in open circuit potential (OCP) situation. As observed, the OCP at equilibrium is different for both samples, due to the presence of Au particles in one of them, which modifies the surface chemistry and electronics. When the samples are

illuminated, AuNPs/TiO_2NCs shows higher absorption than TiO_2NCs as confirmed by the higher photovoltage signal. Besides, the photocurrents at different bias potentials and under illumination (Figure 9B) exhibit an improvement when Au NPs are supported on TiO_2 nanocolumns. This confirms that the presence of gold nanoparticles improves the light absorption when the samples are illuminated with a solar simulator. This can be attributed to the localized surface plasmon resonance (LSPR) exhibited by Au nanoparticles,[48] taking into account that the measurements were carried out under full-spectrum irradiation.

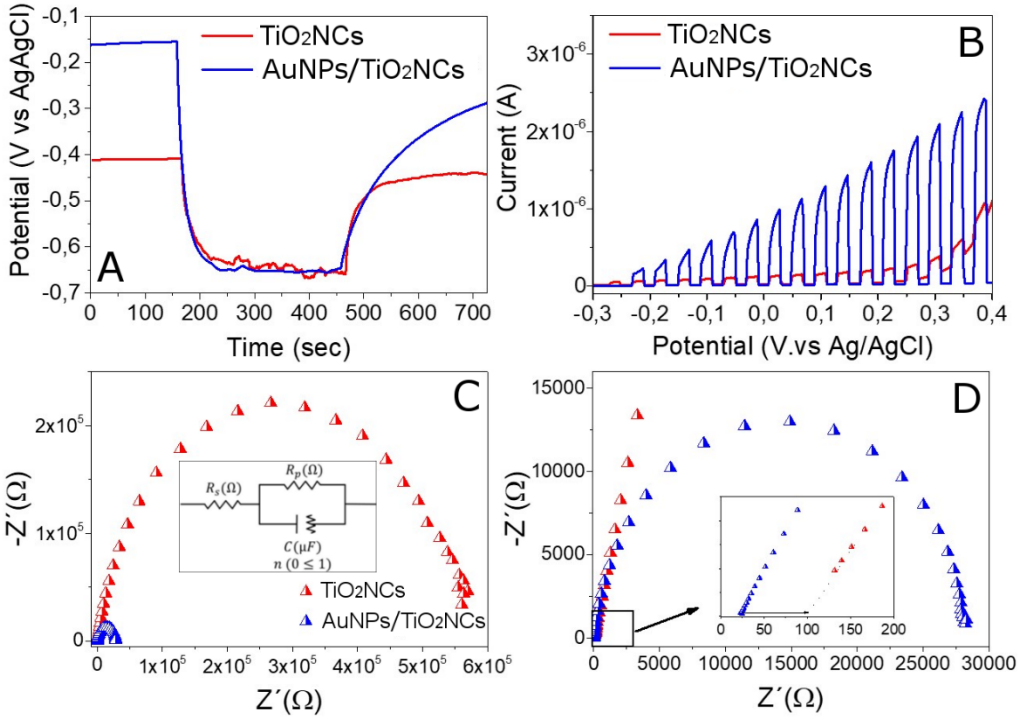

Figure 9. (A) Photovoltage, (B) chopped linear sweep voltammetry, and (C,D) electrochemical impedance spectroscopy at 0.4 V vs Ag / AgCl of TiO_2NCs and AuNPs/TiO_2NCs under irradiation. (C) represents a magnification of the EIS spectrum of AuNPs/TiO_2NCs barely visible in (C). The inset in (D) shows the serial resistance representing the inner material resistance.

Electrochemical impedance spectroscopy (EIS) was performed under irradiation conditions at a bias potential of 0.4 V vs Ag/AgCl (conditions with the highest acquired photocurrent). The resulting Nyquist plots (Figure 9 C and D) show that the resistance of the TiO_2 space charge region greatly decreases when Au NPs are supported on TiO_2NCs (starting from ≈ 600000 Ω to ≈ 30000 Ω). This behavior confirms that, upon gold decoration, the electron recombination

decreases and the charge transfer improves along the semiconductor-electrolyte interface, which explains the better performance of this material as photocatalyst. Additionally, the serial resistance (inset in Figure 9D), which can be attributed to the resistance of the material itself (in addition to the electrolyte resistance and external circuit), presents a lower value in the Au decorated sample, from ≈ 100 to ≈ 25 Ω, as it can be expected in a metal/semiconductor composite with respect to the semiconductor itself and has been frequently ascribed to charge transfer between the semiconductor and metal components.[49]

3. Conclusion

Glancing angle deposition with magnetron sputtering (MS-GLAD) combined with multiple ion cluster source (MICS) has been demonstrated as a powerful technique for the preparation of regular, controlled TiO_2 nanocolumnar structures for photoinduced hydrophilic and self-cleaning applications, and for their further functionalization with metal nanoparticles. MS-GLAD gives rise to metallic titanium columnar structures with regular width and length that after thermal annealing in synthetic air atmosphere are fully oxidized to form TiO_2 nanocolumns that fairly maintain the morphological features of the original metallic ones. Gold decoration by MICS results in well-dispersed Au nanoparticles across the nanocolumns surface with a narrow size distribution centered at ca. 8.5 nm. The obtained nanostructures show photocatalytic activity for the elimination of an organic layer deposited on their surface via the formation of hydroxyl radicals, with the gold-decorated samples resulting in a higher self-cleaning efficiency. Photoelectrochemical measurements have allowed to ascribe the better behavior of the Au-functionalized nanocolumns to a better charge separation at the Au/TiO_2 interface. In addition, wettability studies have shown that the photo-induced hydrophobic-to-hydrophilic transition of the titania nanocolumns is maintained with Au decoration and that the gold-decorated sample gives rise to similar water CA both in the dark and under UV, showing that the opto-electronic modifications induced by gold NPs have a moderate influence of the wettability properties of the samples compared to the roughness

related to the nanocolumnar structure, which tend to increase hydrophobicity in the dark and reduce hydrophilicity under UV iradiation. The obtained results open up interesting implications in the tunability of the properties of nanostructured thin films for this kind of photo-activated applications.

4. Experimental Section

Synthesis of bare and Au NPs-decorated TiO_2 nanocolumn arrays. The aligned 1D TiO_2 nanocolumns have been fabricated in two steps. The first one was the fabrication of Ti metal nanocolumn arrays on silicon wafers by GLAD with magnetron sputtering using the setup and methodology described in detail elsewhere.[35] The sputter gas was argon and the parameters used were 0.15 Pa pressure, 300 W DC discharge power, and a tilt angle of 75° between the substrate and the target. As it has been shown in Fig. 1, the obtained nanocolumns are more vertical than expected if only the geometry of the deposition is considered. This is due to the high kinetic energy of the sputtered atoms (of the order of 10 eV), which is able to induce hyperthermal processes that strongly influence the columnar growth, in particular promoting a dragging mechanism that favors vertical growth. These phenomena are studied in detail in ref. [35]. The second step was the thermal oxidation of the Ti nanocolumn arrays to obtain TiO_2 nanocolumns, for which they were treated at 500 °C for 10 min with a ramp of 10 °C min^{-1} in a synthetic air flow (50 cm^3 min^{-1}), by placing the samples in a quartz tube inside a tubular furnace. After the treatment, the system was let to cool down naturally. Au NPs decoration was carried out by using a multiple ion cluster source (MICS). In the particular case of the present study, the only magnetron that has been used was the one loaded with a pure gold target. Argon was also used as sputtering gas (70 sccm) and the power applied to the magnetron was 4 W. Prior to deposition on the TiO_2 nanocolumns, the Au NPs were deposited on flat SiO_x wafers to measure and adjust their size. After their AFM characterization (see below), the Au NPs were deposited on the TiO_2 nanocolumns placing the substrates perpendicular to the NPs beam.

Physico-chemical characterization. Characterization of sample morphology was performed by means of Scanning Electron Microscopy (SEM) with a FEI Verios 460 Field Emission scanning electron microscope using selective secondary and backscattered electrons detection. An accelerating voltage of 2.0 kV was used in order to obtain high-resolution images while avoiding damage to the sample surface. The height of the Au NPs was precisely measured by atomic force microscopy (AFM), as the height of the NPs measured by AFM is comparable to the diameter measured by transmission electron microscopy.[34] The AFM measurements were performed using the Cervantes AFM System equipped with the Dulcinea electronics from Nanotec Electronica S.L. The images were analyzed using WSxM software.[50] A total of 625 NPs were analyzed in order to extract a mean size distribution. In-situ X-ray diffraction (XRD) of the oxidation process of the metallic Ti nanocolumns was carried out in a Bruker Avance D8 diffractometer equipped with an Anton Paar XRK900 reaction chamber, operational up to 900 °C in a pressure range of 0.001 - 10 bar, and a linear detector LYNXEYE XE. Measurements were taken at every 20 °C from room temperature to 500 °C and then back to room temperature after natural cooldown, using the K_α radiation of copper (λ= 1.54060 Å) with a step size of 0.020°. X-ray photoelectron spectra (XPS) were recorded using a SPECS NAP-XPS system incorporating the DeviSim NAP reaction cell. The spectrometer is equipped with an Al Kα monochromated source (hν = 1486.6 eV), composed of a SPECS XR50 MF x-ray gun and a µ-FOCUS 600 monochromator, and a PHOIBOS 150 NAP 1D-DLD analyzer. X-ray gun power was set to 25 W (1.68 mA emission current and 15 kV). The x-ray analysis spot was set to 300 µm. With this X-ray settings, the intensity of the Ag $3d_{5/2}$ photoemission peak for a Ag sample, recorded at 10 eV pass energy (PE), was 1×10^4 cps and the full width at half maximum (FWHM) was 0.60 eV. Binding energy calibration was made using Au $4f_{7/2}$ (84.01 eV), Ag $3d_{5/2}$ (368.20 eV) and Cu $2p_{3/2}$ (932.55 eV). The survey scans were acquired using 30 eV pass energy, 1 eV step size and 0.5 second dwell times. High resolution spectra were acquired using 10 eV pass energy, 0.1 eV step size and

varying dwell times depending on element concentration. The samples were analyzed at an electron take-off angle normal to the surface with respect to the analyzer. The Si wafer was attached to the holder using double-side sticky tape. No significant signs of charging were observed. The spectra were not charge corrected. Casa XPS was used for data interpretation. Shirley or two-point linear background subtractions were employed depending on background shape. The Au 4f peaks were fitted using a C1s peak for graphitic-like C=C using a LA(1.5,4,60) asymmetric function. The rest of the peaks were fitted using typical GL(30) line shapes: a combination of a Gaussian (70%) and Lorentzian (30%). For the O1s and C1s scans the O1s was constricted to be at 530.4 +/-0.1 eV (characteristic of TiO_2) and the C1s at 285.1+/-0.1 eV (characteristic of adventitious hydrocarbons). All peaks in these C1s and O1s spectra were fitted to have FWHM between 1.3-1.7 eV. Casa XPS sensitivity factors based on Scofield cross-sections were used for atomic percentage quantification analysis (where RSF of C 1s = 1.000).[51]

Functional characterization. Water contact angle (CA) measurements under UV illumination were carried out by a sessile drop method using drops (1 µl) of deionized water at room temperature. The surface energy evaluation system (SEE) from Advex Instruments was used for the acquisition of the drop images and measurement of CA. The initial CA was determined before UV irradiation and after the samples have been kept in the dark for at least one month. Then, the CA evolution under exposure to UV light was obtained by illuminating the samples with a UV fiber-coupled LED (Thorlabs M365FP1, λ_{center} = 365 nm). The light power, as measured in the position of the sample, was fixed at 0.55 mW. The illumination needed to acquire the drop images was carried out with an incandescent bulb with UV filter to avoid uncontrolled light in the UV range. Photocatalytic self-cleaning activities were studied by mean of the solid-state degradation of a stearic acid (SA) layer deposited on the surface of the samples, which was followed by diffuse reflectance infrared (DRIFT) spectroscopy.[43] For that purpose, a 0.2 M solution of stearic acid (Sigma Aldrich) in methanol was prepared.

The TiO_2NCs sample was then coated with that solution by a single dipping with an automatic dip coater at a pulling speed of 10 cm min^{-1}. After drying at 80 °C, DRIFT spectra of the SA-coated sample were recorded in the dark and at regular time intervals during irradiation in a stainless steel chamber with two fluorescent UV lamps (Philips Actinic, λ_{max} = 365 nm) of 6 W each. The degradation of SA was monitored by integrating the bands between 3000 and 2800 cm^{-1}, corresponding to C-H stretching vibrations. Blank experiments with photocatalytic samples in the absence of irradiation and with naked SiO_x substrates under UV irradiation resulted in no decrease of those signals. Indirect hydroxyl radical detection was carried out by means of the hydroxylation reaction of terphthalic acid (TPA) to form the highly fluorescent hydroxyterphthalic acid (HTPA), following the method described by Lavrenčič Stangar and co-workers.[46] For that purpose, the samples were dip-coated (10 cm min^{-1}) into an ethanol/water (2:1) solution containing TPA (0.02 M), 2-hydroxyethylcellulose (HEC, 2.67 g L^{-1}) in alkaline medium (NaOH 0.04 M), which after drying leaves a solid layer of TPA entrapped in HEC on the surface of the sample. The sample was then irradiated with UV light (2 × 6W Philips Actinic, λ_{max} = 365 nm) for a specific period of time, after which the surface was washed with 200 µL of 1:1 water/ethanol, pouring the washate into a microplate for analysis in an Omega microplate reader (BMG Labtech) in fluorescence mode, using 320 and 430 nm as excitation and emission wavelengths, respectively. The procedure was repeated with different irradiation times to obtain a curve of [HTPA] vs. irradiation time that was fitted to the kinetic equation described in the Results and Discussion section.

Electrochemical and photoelectrochemical measurements were performed in a three-electrode glass cell containing a 0.5 M aqueous solution of Na_2SO_3 (pH= 9). TiO_2NCs and AuNPs/TiO_2NCs samples were used as working electrodes. The counter electrode was a platinum wire, and the reference was an Ag/AgCl electrode. Current density (in dark and under illumination) and impedance voltage dependence were measured with a potentiostat-galvanostat PGSTAT302N provided with an integrated impedance module FRAII (10 mV of

modulation amplitude is used at AC frequencies from 1 Hz to 10000 Hz). During the experiment, an argon flow (50 cm^3 min^{-1}) was passed through the cell by bubbling into the solution. A solar simulator (LOT LSH302 Xe lamp with a LSZ389 AM1.5 Global filter) was used as light source.

Acknowledgements

Financial support form the Spanish Ministry of Science, Innovation, and Universities (MICINN) through the projects SOLPAC (ENE2017-89170-R, MCIU/AEI/FEDER, EU), MAT2014-59772-C2-1-P and MAT2014-59772-C2-2-P is gratefully acknowledged. The authors also acknowledge the service from the MiNa Laboratory at IMN funded by Comunidad de Madrid (S2018/NMT-4291 TEC2SPACE), MICINN (CSIC13-4E-1794) and the EU (FEDER, FSE). Also, this work has been funded by the regional government of Madrid and European Structural Funds through their financial support to FotoArt-CM program (S2018/NMT-4367), and from *Fundación Ramon Areces* though the *ArtLeaf* project. M. Barawi thanks MICINN for a *Juan de la Cierva Incorporación* (IJC2019-042430-I) grant.

Received: ((will be filled in by the editorial staff))
Revised: ((will be filled in by the editorial staff))
Published online: ((will be filled in by the editorial staff))

References

[1] P. V. Kamat, *J. Phys. Chem. C* **2012**, *116*, 11849.

[2] F. Fresno, I. J. Villar-García, L. Collado, E. Alfonso-González, P. Reñones, M. Barawi, V. A. de la Peña O'Shea, *J. Phys. Chem. Lett.* **2018**, *9*, 7192.

[3] U. Diebold, *Surf. Sci. Rep.* **2003**, *48*, 53.

[4] M. Grätzel, *J. Photochem. Photobiol. C Photochem. Rev.* **2003**, *4*, 145.

[5] X. Xu, G. Pliego, J. A. Zazo, S. Sun, P. García-Muñoz, L. L. He, J. A. Casas, J. J.

Rodriguez, *Crit. Rev. Environ. Sci. Technol.* **2017**, *47*, 1.

[6] Y. Boyjoo, H. Sun, J. Liu, V. K. Pareek, S. Wang, *Chem. Eng. J.* **2017**, *310*, 537.

[7] F. Han, L. Zhu, Z. Huang, Z. Zhou, *J. Phys. Chem. Lett.* **2020**, *11*, 7590.

[8] J. K. Stolarczyk, S. Bhattacharyya, L. Polavarapu, J. Feldmann, *ACS Catal.* **2018**, *8*, 3602.

[9] M. T. Spitler, M. A. Modestino, T. G. Deutsch, C. X. Xiang, J. R. Durrant, D. V. Esposito, S. Haussener, S. Maldonado, I. D. Sharp, B. A. Parkinson, D. S. Ginley, F. A. Houle, T. Hannappel, N. R. Neale, D. G. Nocera, P. C. McIntyre, *Sustain. Energy Fuels* **2020**, *4*, 985.

[10] M. Melchionna, P. Fornasiero, *ACS Catal.* **2020**, *10*, 5493.

[11] M. Konar, B. Roy, T. Govindaraju, *Adv. Mater. Interfaces* **2020**, *7*.

[12] I. P. Parkin, R. G. Palgrave, **2005**, 1689.

[13] L. Zhang, R. Dillert, D. Bahnemann, M. Vormoor, *Energy Environ. Sci.* **2012**, *5*, 7491.

[14] S. Banerjee, D. D. Dionysiou, S. C. Pillai, *Appl. Catal. B Environ. Environ.* **2015**, *176–177*, 396.

[15] V. Rodríguez-González, S. Obregón, O. A. Patrón-Soberano, C. Terashima, A. Fujishima, *Appl. Catal. B Environ.* **2020**, *270*, 118853.

[16] C. Zhang, Y. Li, D. Shuai, Y. Shen, D. Wang, *Chem. Eng. J.* **2019**, *355*, 399.

[17] C. Weiss, M. Carriere, L. Fusco, I. Capua, J. A. Regla-Nava, M. Pasquali, J. A. Scott, F. Vitale, M. A. Unal, C. Mattevi, D. Bedognetti, A. Merkoçi, E. Tasciotti, A. Yilmazer, Y. Gogotsi, F. Stellacci, L. G. Delogu, *ACS Nano* **2020**, *14*, 6383.

[18] M. Miyauchi, K. Sunada, K. Hashimoto, *Catalysts* **2020**, *10*, 1.

[19] J. Chang, L. Zhang, P. Wang, *Environ. Sci. Nano* **2018**, *5*, 811.

[20] I. Ali, M. Suhail, Z. A. Alothman, A. Alwarthan, *RSC Adv.* **2018**, *8*, 30125.

[21] R. Alvarez, J. M. García-Martín, M. MacÍas-Montero, L. Gonzalez-Garcia, J. C. González, V. Rico, J. Perlich, J. Cotrino, A. R. González-Elipe, A. Palmero,

Nanotechnology **2013**, *24*.

[22] A. Vitrey, R. Alvarez, A. Palmero, M. U. González, J. M. García-Martín, *Beilstein J. Nanotechnol.* **2017**, *8*, 434.

[23] G. Troncoso, J. M. García-Martín, M. U. González, C. Morales, M. Fernández-Castro, J. Soler-Morala, L. Galán, L. Soriano, *Appl. Surf. Sci.* **2020**, *526*.

[24] Z. Hu, J. M. Garcia-Martin, Y. Li, L. Billot, B. Sun, F. Fresno, A. García-Martín, M. U. González, L. Aigouy, Z. Chen, J. M. García-Martín, Y. Li, L. Billot, B. Sun, F. Fresno, A. García-Martín, M. U. González, L. Aigouy, Z. Chen, *ACS Appl. Mater. Interfaces* **2020**, *12*, 5979.

[25] B. N. Reinecke, K. P. Kuhl, H. Ogasawara, L. Li, J. Voss, F. Abild-pedersen, A. Nilsson, T. F. Jaramillo, *Surf. Sci.* **2016**, *650*, 24.

[26] L. Martínez, M. Díaz, E. Román, M. Ruano, D. Llamosa P., Y. Huttel, *Langmuir* **2012**, *28*, 11241.

[27] D. Llamosa, M. Ruano, L. Martínez, A. Mayoral, E. Roman, M. García-Hernández, Y. Huttel, *Nanoscale* **2014**, *6*, 13483.

[28] A. Mayoral, D. Llamosa, Y. Huttel, *Chem. Commun.* **2015**, *51*, 8442.

[29] L. Martínez, A. Mayoral, M. Espiñeira, E. Roman, F. J. Palomares, Y. Huttel, *Nanoscale* **2017**, *9*, 6463.

[30] H. Haberland, M. Mall, M. Moseler, Y. Qiang, T. Reiners, Y. Thurner, *J. Vac. Sci. Technol. A Vacuum, Surfaces Film.* **1994**, *12*, 2925.

[31] Y. Huttel, Ed., *Gas-Phase Synthesis of Nanoparticles*, Wiley-VCH Verlag GmbH, **2017**.

[32] D. Llamosa Pérez, A. Espinosa, L. Martínez, E. Román, C. Ballesteros, A. Mayoral, M. García-Hernández, Y. Huttel, *J. Phys. Chem. C* **2013**, *117*, 3101.

[33] M. Ruano, M. Díaz, L. Martínez, E. Navarro, E. Román, M. García-Hernandez, A. Espinosa, C. Ballesteros, R. Fermento, Y. Huttel, *Phys. Chem. Chem. Phys.* **2013**, *15*,

316.

[34] M. Díaz, L. Martínez, M. M. Ruano, D. Llamosa P, E. Román, M. García-Hernandez, C. Ballesteros, R. Fermento, A. Cebollada, G. Armelles, G. Armelles, Y. Huttel, *J. Nanoparticle Res.* **2011**, *13*, 5321.

[35] R. Alvarez, J. M. Garcia-Martin, A. Garcia-Valenzuela, M. Macias-Montero, F. J. Ferrer, J. Santiso, V. Rico, J. Cotrino, A. R. Gonzalez-Elipe, A. Palmero, *J. Phys. D. Appl. Phys.* **2015**, *49*, 45303.

[36] U. Diebold, T. E. Madey, *Surf. Sci. Spectra* **1996**, *227*, 227.

[37] N. Sakai, A. Fujishima, T. Watanabe, K. Hashimoto, *J. Phys. Chem. B* **2003**, *107*, 1028.

[38] M. Miyauchi, N. Kieda, S. Hishita, T. Mitsuhashi, A. Nakajima, T. Watanabe, K. Hashimoto, *Surf. Sci.* **2002**, *511*, 401.

[39] X. Zhang, M. Jin, Z. Liu, D. A. Tryk, S. Nishimoto, T. Murakami, A. Fujishima, *J. Phys. Chem. C* **2007**, *111*, 14521.

[40] J. Shondo, S. Veziroglu, D. Stefan, Y. K. Mishra, T. Strunskus, F. Faupel, O. C. Aktas, *Appl. Surf. Sci.* **2021**, *537*, 147795.

[41] Y. Paz, Z. Luo, L. Rabenberg, A. Heller, *J. Mater. Res.* **1995**, *10*, 2842.

[42] Y. Paz, A. Heller, *J. Mater. Res.* **1997**, *12*, 2759.

[43] A. Mills, A. Lepre, N. Elliott, S. Bhopal, I. P. Parkin, S. A. O'Neill, *J. Photochem. Photobiol. A Chem.* **2003**, *160*, 213.

[44] T. Minabe, D. A. Tryk, P. Sawunyama, Y. Kikuchi, K. Hashimoto, A. Fujishima, *J. Photochem. Photobiol. A Chem.* **2000**, *137*, 53.

[45] P. Sawunyama, L. Jiang, A. Fujishima, K. Hashimoto, *J. Phys. Chem. B* **1997**, *101*, 11000.

[46] U. Černigoj, M. Kete, U. L. Štangar, *Catal. Today* **2010**, *151*, 46.

[47] D. Barreca, G. Carraro, A. Gasparotto, C. MacCato, F. Rossi, G. Salviati, M. Tallarida, C. Das, F. Fresno, D. Korte, U. L. Štangar, M. Franko, D. Schmeisser, *ACS Appl.*

Mater. Interfaces **2013**, *5*, 7130.

[48] K. L. Kelly, E. Coronado, L. L. Zhao, G. C. Schatz, *J. Phys. Chem. B* **2003**, *107*, 668.

[49] L. Collado, A. Reynal, F. Fresno, M. Barawi, C. Escudero, V. Perez-Dieste, J. M. Coronado, D. P. Serrano, J. R. Durrant, V. A. de la Peña O'Shea, *Nat. Commun.* **2018**, *9*, 4986.

[50] I. Horcas, R. Fernández, J. M. Gómez-Rodríguez, J. Colchero, J. Gómez-Herrero, A. M. Baro, *Rev. Sci. Instrum.* **2007**, *78*.

[51] J. H. Scofield, *J. Electron Spectros. Relat. Phenomena* **1976**, *8*, 129.

Glancing angle deposition with magnetron sputtering (MS-GLAD) has been demonstrated as a powerful technique for the preparation of regular, controlled TiO_2 nanocolumnar structures with photoinduced self-cleaning and hydrophilic properties. Further functionalization with Au nanoparticles by a multiple ion cluster source (MICS) improves photocatalytic activity and allows to switch the arrays from hydrophilic to hydrophobic under UV irradiation.

Fernando Fresno,* María U. González, Lidia Martínez, Marcial Fernández-Castro, Mariam Barawi, Ignacio J. Villar-García, Jimena Soler-Morala, Patricia Reñones, Mónica Luna, Yves Huttel,* Víctor A. de la Peña O'Shea,* José M. García-Martín*

Photo-induced self-cleaning and wettability in TiO_2 nanocolumn arrays obtained by glancing-angle deposition with sputtering

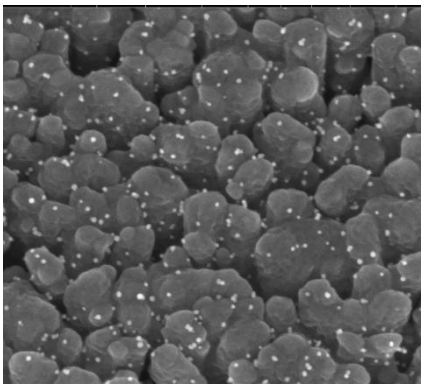

Supporting Information

Photo-induced self-cleaning and wettability in TiO_2 nanocolumn arrays obtained by glancing-angle deposition with sputtering

Fernando Fresno, María U. González, Lidia Martínez, Marcial Fernández-Castro, Mariam Barawi, Ignacio J. Villar-García, Jimena Soler-Morala, Patricia Reñones, Mónica Luna, Yves Huttel,* Víctor A. de la Peña O'Shea,* José M. García-Martín**

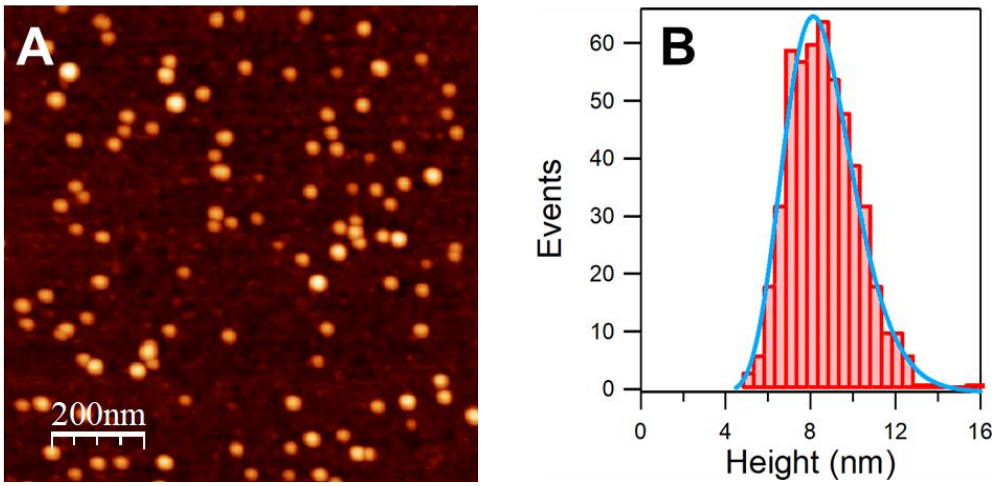

Figure S1. (A) AFM image of model Au NPs deposited on a SiO_x substrate. (B) Height distribution extracted from the analysis of the AFM images.

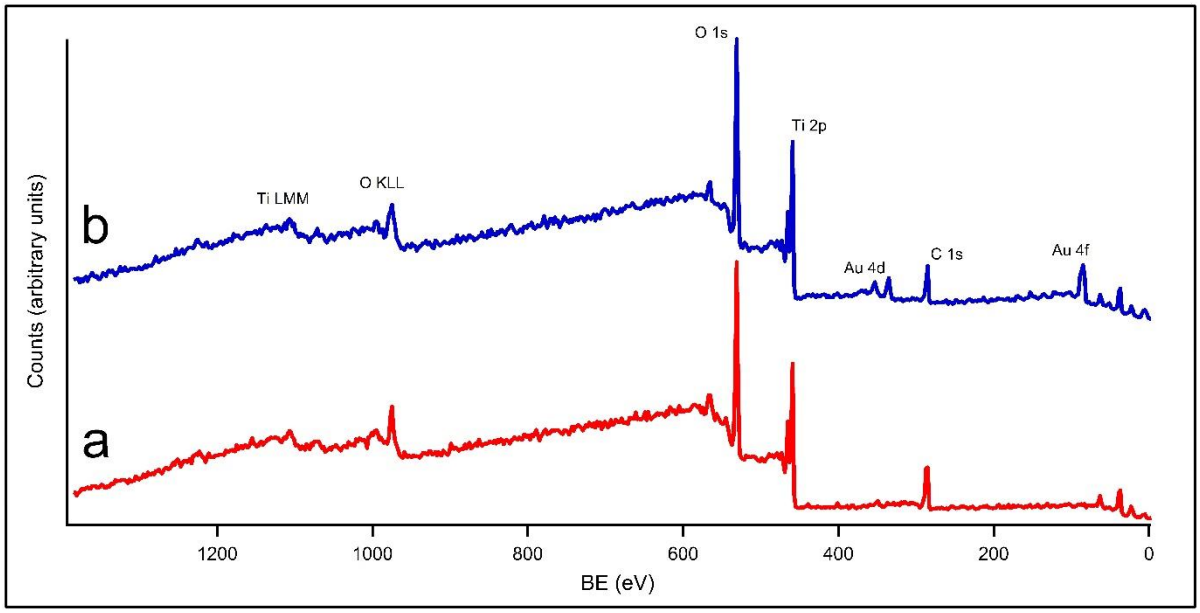

Figure S2. Survey XPS scans of TiO_2NCs (a) and AuNPs/TiO_2NCs (b).

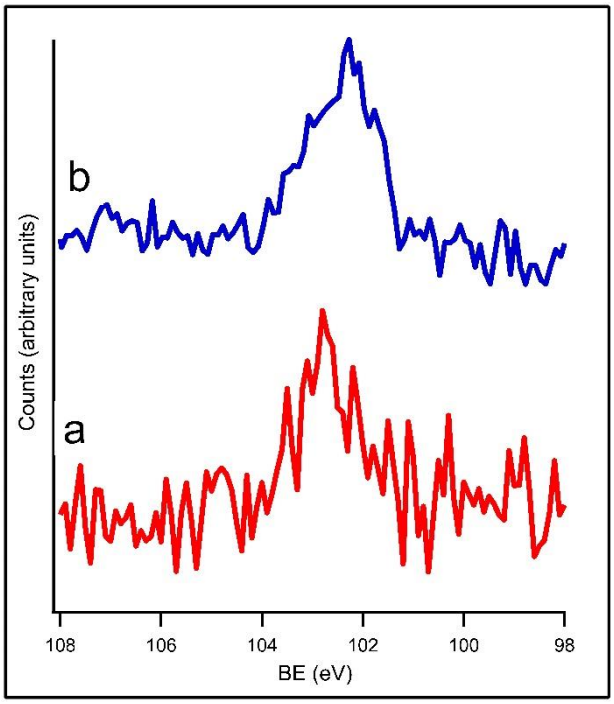

Figure S3. High-resolution X-ray photoelectron spectra of TiO_2NCs (a) and AuNPs/TiO_2NCs (b) samples in the Si2p region.

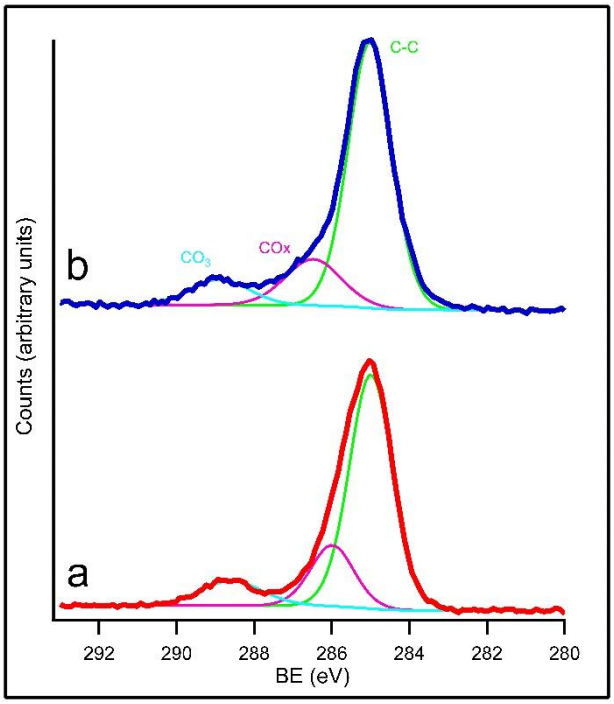

Figure S4. High-resolution X-ray photoelectron spectra of TiO_2 NCs (a) and AuNPs/TiO_2NCs (b) samples in the C1s region.